



1 **Novel aerosol extinction coefficients and lidar ratios over the ocean from**
2 **CALIPSO-CloudSat: Evaluation and global statistics**

3

4

5 David Painemal^{1,2}, Marian Clayton^{1,2}, Richard Ferrare², Sharon Burton², Damien Josset³, and

6 Mark Vaughan²

7 ¹Science Systems and Applications Inc., Hampton, VA, 23666 USA

8 ²NASA Langley Research Center, Hampton, VA, 23666 USA

9 ³US Naval Research Laboratory Stennis Space Center, MS, 39529, USA

10

11 *Correspondence to:* David Painemal (david.painemal@nasa.gov)

12

13 **Abstract.** Aerosol extinction coefficients (σ_a) and lidar ratios (LR) are retrieved over the ocean
14 from CALIOP attenuated backscatter profiles by solving the lidar equation constrained with
15 aerosol optical depths (AOD) derived by applying the Synergized Optical Depth of Aerosols
16 (SODA) algorithm to ocean surface returns measured by CALIOP and CloudSat's Cloud Profiling
17 Radar. σ_a and LR are retrieved for two independent scenarios that require somewhat different
18 assumptions: a) a single homogeneous atmospheric layer (1L) for which the LR is constant with
19 height, and b) a vertically homogeneous layer with a constant LR overlying a marine boundary
20 layer with a homogenous LR fixed at 25 sr (2-layer method, 2L). These new retrievals differ from
21 the standard CALIPSO version 4.1 (V4) product, as the CALIOP-SODA method does not rely on
22 an aerosol classification scheme to select LR. CALIOP-SODA σ_a and LR are evaluated using
23 airborne high spectral resolution lidar (HSRL) observations over the northwest Atlantic. CALIOP-
24 SODA LR (1L and 2L) positively correlates with its HSRL counterpart (linear correlation
25 coefficient $r > 0.67$), with a negative bias smaller than 13.2%, and a good agreement for σ_a (r
26 ≥ 0.78) with a small negative bias ($\leq -9.2\%$). Furthermore, a global comparison of optical depths
27 derived by CALIOP SODA and CALIPSO V4 reveals substantial differences over regions
28 dominated by dust and smoke, in qualitative agreement with previously reported discrepancies
29 between MODIS and CALIPSO AOD.

30 Global maps of CALIOP-SODA LR feature high values over littoral zones, consistent with
31 expectations of continental aerosol transport offshore. In addition, seasonal transitions associated



1 with biomass burning during June to October over the southeast Atlantic are well reproduced by
2 CALIOP-SODA LR.

3

4 **1. Introduction**

5 Advances in our understanding of the 3D structure of atmospheric aerosols have been greatly
6 accelerated with the advent of the Cloud-Aerosol Lidar with Orthogonal Polarization (CALIOP),
7 onboard the Cloud-Aerosol Lidar and Infrared Pathfinder Satellite Observation (CALIPSO,
8 Winker et al., 2009; 2010, 2013). CALIOP has provided the first global view of aerosol distribution
9 in the boundary layer and free troposphere (Winker et al., 2013), progressed our knowledge of the
10 long-range transport of dust (e.g. Liu et al., 2008; Uno et al., 2010; Yu et al., 2015) and smoke
11 (e.g. de Laat et al., 2012; Das et al., 2017; Khaykin et al., 2018), and facilitated the evaluation of
12 chemical transport models (Nowottnick et al., 2015; Koffi et al., 2016), among many other
13 accomplishments in the area of aerosol and cloud research.

14 CALIOP estimates aerosol extinction coefficients on a global scale with an unprecedented
15 vertical detail. The undetermined problem of solving the lidar equation with two physical
16 unknowns, the aerosol extinction and backscatter coefficients, is addressed in the CALIPSO
17 algorithm by relating both variables via an extinction-to-backscatter ratio, or lidar ratio (LR). This
18 standard technique (e.g. Fernald, 1984) expresses the lidar equation in terms of only one unknown,
19 if LR is prescribed. As aerosol types can be related to specific values of lidar ratios (e.g. Müller
20 et al., 2007), the CALIPSO algorithm utilizes predefined LR assigned to a number of aerosol types,
21 which in turn, are identified using the CALIPSO automated aerosol typing algorithm (Omar et al.,
22 2009; Kim et al., 2018). Thus, the quality of CALIOP retrievals will depend on how well the actual
23 lidar ratios match the pre-tabulated values and to what extent the aerosol typing algorithm properly
24 classifies aerosols. Another source of uncertainty is the detectability limits of the CALIPSO
25 algorithm, which prevents retrieving aerosol properties for tenuous aerosol layers (Rogers et al.,
26 2014; Thorsen et al., 2017). For instance, Toth et al. (2018) found that no aerosol was detected
27 within ~71% of the CALIOP profiles measured during daytime and ~41% of the nighttime
28 measurements. More aerosol detection during nighttime is explained by the absence of solar
29 background noise, which leads to a significantly better signal to noise ratio. The aforementioned
30 factors likely explain discrepancies between CALIOP and other remote sensing datasets such as



1 those from the MODerate resolution Imaging Spectroradiometer (MODIS) and AERONET (e.g.
2 Redemann et al., 2012; Schuster et al., 2012).

3 Uncertainty reduction in the selection of LR can be attained by constraining the lidar
4 equation solution with an independent estimate of aerosol optical depth (AOD). This implies the
5 minimization of the error between the retrieved AOD (estimated from the retrieved extinction
6 coefficient coefficient) and the target AOD by iteratively adjusting LR. Burton et al. (2010) utilize
7 AOD from the MODIS instruments on board both Aqua and Terra satellites for estimating aerosol
8 extinction from CALIOP for cases in which AOD exceeds 0.15 (0.2) over the ocean (land).
9 Similarly, Royer et al. (2010) applied an equivalent method for estimating LR and extinction
10 coefficients over the Po Valley in Italy. Although CALIOP-MODIS retrievals in Burton et al.
11 (2010) tend to compare better with airborne measurements relative to CALIPSO standard product
12 (Version 2), MODIS AOD is limited to daytime, and MODIS and CALIOP differ in their along-
13 track spatial resolution. These previous studies have proven the value of counting on independent
14 CALIOP retrievals for evaluating CALIPSO's standard data products.

15 In this contribution, we present a new method in which CALIOP-based lidar ratios and
16 aerosol extinction coefficients over the non-polar oceans are obtained by constraining the retrievals
17 with AOD derived from cross-calibrated CALIOP and CloudSat Cloud Profiling Radar (CPR)
18 surface echos, using the Synergized Optical Depth of Aerosols (SODA) product (Josset et al.,
19 2008). SODA AOD is a suitable dataset, as it is collocated with CALIOP by definition and
20 retrievals are possible during both daytime and nighttime for the period 2006-2011. After
21 November 2011 SODA is only available for daytime, as CloudSat has operated in daylight-only
22 operations mode to conserve power (Gravseth and Piepe, 2013). Our goal is to provide an
23 independent CALIOP dataset that can be used for evaluating specific aspects of the CALIPSO
24 Science Team product, as well as for investigating aerosol-related topics in climate research. We
25 first summarize the algorithm and evaluate the new retrievals against state-of-the-art aerosol
26 observations from the NASA Langley airborne High Spectral Resolution Lidar-1 (HSRL, Sections
27 3 and 4). Next, we compare the CALIOP-SODA extinction coefficient and AOD with their
28 CALIPSO Science Team Version 4 counterparts. Lastly, we present global maps of lidar ratio and
29 marine boundary layer aerosol optical depth, and provide a physical interpretation for the regional
30 patterns derived from CALIOP-SODA.

31



1 2. Dataset

2 2.1. CALIOP

3 Version 4.1 (V4) CALIOP elastic backscatter lidar measurements at 532 nm and 1064 nm
4 are utilized in this work. For the derivation of CALIOP-SODA retrievals, we use Level 1 lidar
5 attenuated backscatter and the Level 2 Vertical Feature Mask product, with a 333 m horizontal
6 resolution below 8.2 km. CALIOP V4 aerosol extinction coefficients and AOD estimates are taken
7 from the Level 2 Aerosol Profile product at 5 km horizontal resolution. For comparing CALIOP
8 SODA and V4 products, we follow the procedure outlined in Koffi et al. (2016): where the VFM
9 feature classification flags indicate regions of clear air, we set the corresponding extinction
10 coefficients to zero. While these regions are labeled as ‘clear air’, they are simultaneously assumed
11 to be populated by highly diffuse aerosols that lie well below the CALIOP layer detection
12 threshold.

13

14 2.2. SODA aerosol optical depth

15 SODA uses the relationship between CALIOP (532 nm and 1064 nm) and CPR (3.1 mm, 94 GHz)
16 surface return signals, along with a correction for the atmospheric transmission at the radar wavelength,
17 to derive AOD at the lidar wavelengths. In short, SODA estimates of AOD rely on the radar-to-lidar
18 ocean surface scattering cross-calibration for cloud-free columns (Josset et al., 2008, 2010).
19 Consequently, SODA can provide a cloud-free AOD without having to rely on an accurate assignment
20 of a particular aerosol type with an appropriate lidar ratio. In addition, the algorithm does not depend
21 on pre-determined aerosol models with a specific particle size distributions and refractive indexes,
22 unlike MODIS. SODA AOD Version 2, based on CALIPSO Version 3 (V3), is developed at the
23 ICARE data and services center (<http://www.icare.univ-lille1.fr>) in Lille (France) under the auspices
24 of the CALIPSO mission and supported by the French National Centre for Space Studies (CNES).
25 Josset et al. (2013) estimate a systematic error in SODA AOD of 0.015 and 0.059, respectively,
26 for nighttime and daytime AOD. In addition, good agreement between SODA and MODIS has been
27 reported in Josset et al. (2010, 2015), while Dawson et al. (2015) reports a root-mean-square-error
28 of 0.03 between SODA and AERONET AOD and $r = 0.59$ for AERONET sites near the coast.
29 Further, we also evaluate SODA AOD with HSRL data in Section 4, and compare SODA and MODIS
30 AOD over the global ocean in Section 6. While 1064 nm SODA AOD is also utilized in this study,
31 caution needs to be exercised when using the 1064 nm SODA data due to uncertainty calibrations in
32 CALIPSO V3 (Vaughan et al., 2010).



1

2 **2.3.HSRL**

3 CALIOP retrievals are evaluated against airborne measurements by the NASA Langley
 4 High Spectral Resolution Lidar (HSRL, Hair et al., 2008) at 532 nm. The instrument allows for
 5 the independent determination of aerosol extinction and backscatter coefficients at 532 nm (and
 6 thus, lidar ratio) using the HSRL technique (Eloranta, 2005). As HSRL measurements at 1064 nm
 7 are limited to attenuated backscatter, similar to CALIOP, only 532 nm HSRL retrievals will be
 8 utilized in this study. The data used in this study were acquired August 11–27, 2010 while the
 9 HSRL conducted a dedicated CALIPSO validation campaign over the Caribbean Sea (Burton et
 10 al., 2013; Rogers et al., 2014). As required for all HSRL-CALIPSO validation measurements, the
 11 HSRL flight paths during this campaign were spatially matched with coincident CALIPSO ground
 12 tracks (Rogers et al., 2014).

13

14 **3. Derivation of aerosol extinction coefficient and lidar ratio**

15 The method for deriving aerosol extinction coefficient (σ_a) and lidar ratio (LR) is based on
 16 Fernald (1984) applied to the CALIOP attenuated backscatter, and is briefly summarized in the
 17 following. For CALIOP, the lidar equation is expressed in terms of height z (range) as:

$$18 \quad \beta_{att}(z) = (\beta_m(z) + \beta_a(z)) \cdot \exp\left(-2 \int_0^z (\sigma_m(z') + \sigma_a(z')) dz'\right) \quad (1)$$

19 Where β_{att} corresponds to the CALIOP total attenuated backscattering cross section, β_m and β_a
 20 denote the molecular (m) and aerosol (a) backscatter coefficients, and σ_m and σ_a are the molecular
 21 and aerosol extinction coefficients. Since the molecular contribution can be accurately estimated
 22 using atmospheric profiles from numerical weather models, the two unknowns are $\beta_a(z)$ and
 23 $\sigma_a(z)$. Equation (1) can be reduced to one unknown by relating extinction and backscatter
 24 coefficient via their lidar ratio, that is

$$25 \quad LR = \frac{\sigma_a(z)}{\beta_a(z)}. \quad (2)$$

26 It follows that eq. (1) can be expressed in terms of LR and β_m as:

$$27 \quad \beta_{att}(Z) = (\beta_m(z) + \beta_a(z)) \cdot \exp\left(-2 \int_0^z (\sigma_m(z') + LR \cdot \beta_a(z')) dz'\right) \quad (3)$$

28 β_m is estimated as a function of air density (from the Goddard Earth Observing System
 29 Model, Version 5 GEOS-5), and effect of ozone attenuation is accounted for in σ_m following



1 Vaughan et al. (2005). $\beta_a(z)$ and $\sigma_m(z)$ are, thus, estimated from Eq. (3) as in Fernald (1984),
2 assuming a constant value of LR with height. The LR selection is physically constrained by
3 comparing the retrieved aerosol optical depth ($AOD_{ret} = \int_0^z \sigma_a(z') dz'$) with SODA AOD
4 (AOD_{SODA}), and LR is iteratively adjusted until the retrieved AOD matches the SODA AOD to
5 within 0.001 or less (i.e., when $|AOD_{ret} - AOD_{SODA}| \leq 0.001$).

6 We also consider an additional scenario for solving the lidar equation, which consists of
7 treating the atmospheric column as two layers, that is., the marine atmospheric boundary layer
8 (MBL) and a second aerosol layer of as-yet-undetermined composition. This method is intended
9 to better capture specific events with two predominant aerosol types, namely, smoke over marine
10 aerosols and dust over marine aerosols, which are particularly frequent over the Atlantic Ocean.
11 The LR for the MBL is assumed constant at 25 sr, as suggested by HSRL measurements over the
12 ocean (Burton et al., 2012; 2013). This lidar ratio is slightly higher than the one compiled by Kim
13 et al. (2018) for maritime aerosols (23 sr). $\sigma_a(z)$ and the upper layer LR are iteratively calculated
14 using the Fernald method with the constraint provided by AOD_{SODA} , and LR =25 sr in MBL. MBL
15 height is computed by applying the bulk Richardson number method (McGraw-Spangler and
16 Molod, 2014) to GEOS-5 atmospheric fields.

17 In sum, aerosol extinction profiles and lidar ratio are calculated using one of two
18 independent assumptions: either a single homogeneous layer (1L method), or a two-layer
19 atmosphere with a prescribed LR=25 sr in the boundary layer and a single free tropospheric LR,
20 which is estimated during the iterative process (2L method).

21 The CALIOP attenuated backscatter at 333 m resolution is taken from the Level 1
22 CALIPSO product. Before retrieving LR and σ_a , three contiguous 333-m lidar attenuated
23 backscatter samples are averaged to achieve a 1 km along-track resolution. Similarly, SODA AOD
24 retrieved at 333m is averaged to 1 km resolution. In addition, the Feature Classification Mask
25 product is utilized for identifying cloudy pixels and cases with fully attenuated signal, in which
26 CALIOP-SODA retrievals are not possible.

27

28 **4. CALIOP-SODA evaluation with airborne HSRL measurements**

29 CALIOP-SODA retrievals of aerosol extinction coefficient, lidar ratio and AOD are
30 evaluated using eight flights during August 2010 over the western Atlantic, for the domain
31 bounded by 70°W-55°W and 13°N-35°N (Figure 1a). CALIOP-SODA is spatially averaged to



1 match the nominal 5 km horizontal resolution of CALIPSO V4, and only samples with 5-km cloud-
2 free scenes are retained. Both CALIPSO V4 and CALIOP-SODA are then spatially collocated
3 with the aircraft track (Figure 1) for samples with a temporal mismatch of less than 90 minutes
4 (Rogers et al., 2014). Lastly, satellite and airborne observations are spatially averaged to a common
5 0.5 ° resolution (in latitude). Approximately 42 and 46 0.5°-samples were collocated with HSRL
6 (CALIOP-SODA and CALIOP, respectively).

7 The HSRL measurements during Caribbean 2010 were characterized by the presence of
8 dust, dust mixed with maritime aerosols, and continental pollution; the occurrence of pure
9 maritime aerosols was confined to the boundary layer (Burton et al., 2013). This aerosol typing is
10 manifested in a lidar ratio of 25 sr below 500 m, and a linear increase with height that reaches
11 values of 40-45 sr in the free troposphere (Fig. 1b). These measurements also provide justification
12 for the use of a lidar ratio of 25 sr in the boundary layer for the 2L method. Before evaluating
13 aerosols extinction coefficients and lidar ratios, we compare SODA AODs and CALIOP V4 AODs
14 against their HSRL counterparts (Fig. 2a). In general, both CALIOP-based retrievals correlate
15 well with the HSRL, with a slightly higher correlation for SODA, and absolute bias between 10-
16 17%), with SODA (CALIOP V4) underestimating (overestimating) AOD. Linear fits of SODA
17 and V4 AOD relative to HSRL (red and blue lines in Fig. 2a) indicate that the SODA bias is
18 relatively constant with AOD whereas a V4 AOD overestimate tends to increase with AOD
19 especially during nighttime. Nighttime and daytime correlations remain approximately the same
20 for both CALIOP V4 and SODA. However, V4 linear correlation coefficient for AOD < 0.3 are
21 slightly lower for daytime ($r = 0.78$) than nighttime ($r = 0.94$), whereas SODA daytime/nighttime
22 correlations for low AOD remain high ($r \geq 0.93$). The reduced daytime correlation for CALIOP
23 V4 is expected as the reduced signal to noise ratio due to the solar background signal hampers the
24 algorithm's ability to detect and classify aerosols. Finally, in terms of the root-mean-square error
25 (RMSE), SODA RMSE (24.2% relative to the mean) is smaller than that for CALIOP V4 (31.2%,
26 Table 1).

27 The evaluation of CALIOP-SODA lidar ratio and aerosol extinction coefficient is
28 summarized in the following. For LR, we use the column-effective lidar ratio, calculated as:

29

$$LR_{HSRL} = \frac{\sum_{z=z_0}^{6km} \sigma_a(z)}{\sum_{z=z_0}^{6km} \beta_a(z)} \quad (4)$$



1 For evaluating CALIOP SODA 1L LR, LR_{HSRL} in eq. (4) is estimated using the last range bin above
2 the ocean surface (37.8 m) as the lower bound, z_0 . In addition, the comparison between CALIPSO
3 SODA 2L LR and LR_{HSRL} is performed by recomputing LR_{HSRL} using the MBL height for z_0 in eq.
4 4. Since valid HSRL extinctions retrievals are only derived for heights above 270 m from the
5 surface, we have assumed a constant extinction coefficient for the layer below 270 m, with values
6 taken from the lowest height with available retrievals (~ 270 m). The comparison depicted in Fig.
7 2b, yields $r = 0.67$ - 0.74 between both CALIOP-SODA methods (1L and 2L) and HSRL, with a
8 negative mean bias smaller than 13%, and RMSE of up to 8.1 sr (Figure 2b and Table 2).

9 Mean vertically-resolved aerosol extinction coefficients from SODA, CALIOP V4, and
10 HSRL are depicted in Figure 3a and b for daytime and nighttime observations, respectively. The
11 agreement between HSRL (red) and CALIOP-SODA 1L and 2L (overlapped gray and black) is
12 remarkable throughout the lower troposphere, with a maximum overestimation of 0.027 km^{-1}
13 (50%) near 500 m. CALIOP-SODA 1L and 2L yield identical results, which is likely the effect of
14 a shallow marine boundary layer (<500 m). In contrast, CALIOP V4 (blue) consistently
15 overestimates the airborne measurements for heights below 1 km during both daytime and
16 nighttime, with magnitudes up to 0.102 km^{-1} (100%) relative to the HSRL during nighttime and
17 0.078 km^{-1} (140%) during the day. This overestimate is explained by the CALIPSO V4 constant
18 lidar ratio of 37 sr for dusty marine aerosol, which is generally higher than the lidar ratio retrieved
19 by both the HSRL and SODA for Caribbean 2010 (Figure 2b). Interestingly, both CALIOP-SODA
20 and CALIOP V4 correlate well with the HSRL, with correlations around 0.80 (Table 3). The
21 RMSE for CALIOP V4 is also higher than that for CALIOP-SODA especially below 1 km, with
22 maxima around 0.12 km^{-1} (155%) and 0.06 km^{-1} (83%) for CALIOP V4 and CALIOP-SODA,
23 respectively (Fig 3c). Aerosol extinction coefficient statistics for the atmospheric column below
24 3.0 km (Table 2) corroborate the overall smaller bias and RSME of CALIOP-SODA relative to
25 V4.

26

27 5. Global analysis

28 5.1. Comparison between CALIOP-SODA and CALIOP-V4

29 Five months of collocated SODA and CALIOP V4 Level 2 data during June-October 2010
30 were compared over non-polar oceanic regions with the goal of identifying main differences in
31 aerosol extinction coefficient profiles. This period was selected because of the high global



1 climatological AOD observed over the ocean by CALIOP (e.g. Yu et al., 2010). We first averaged
2 1km CALIOP-SODA to the V4 Level 2 nominal resolution (5km). Then, CALIOP-SODA and
3 CALIOP V4 retrievals were further reduced by averaging the retrievals to a common 25 km
4 resolution. Lastly, we reduced the potential effect of overcast scenes in the retrievals by limiting
5 the comparison to 25-km samples with less than 2/3 (67%) of cloudy coverage. Cloud cover was
6 derived from the 333 m Vertical Feature Mask and determined as the ratio between profiles with
7 at least one cloudy feature in the atmospheric column to the total. To circumvent CALIOP's
8 narrow field of view, we calculated the statistics in $6^\circ \times 3^\circ$ (longitude x latitude) grids.

9 We first focus on the AOD difference (Δ AOD) between CALIOP V4 and SODA at 532
10 nm and 1064 nm, for day and nighttime (Figure 4). Daytime 532 nm Δ AOD maps reveal higher
11 V4 AOD than SODA for the northeast Atlantic (NEA) and the Indian Ocean (IO), whereas V4
12 AOD is smaller than SODA over the southeast Atlantic (SEA) and over vast regions of the open
13 ocean. As will be discussed in Section 6, these differences are similar to those observed between
14 CALIOP V3 and MODIS (Redemann et al., 2012). Overall, nighttime differences in 532 nm AOD
15 appear to diminish especially for the SEA and the northwest Pacific (NWP), while the positive
16 Δ AOD remains high over IO and NEA.

17 We also show Δ AOD for the 1064 nm channel in Figure 4 (lower panels). The largest
18 Δ AOD values are mostly confined to the NEA and IO domains, with higher values for SODA
19 AOD, while nighttime Δ AOD are similar to its daytime counterpart.

20 Matched CALIOP-SODA and CALIOP V4 mean vertical profiles of aerosol extinctions
21 over the regions defined in Figure 4 (black boxes) are shown in Figs. 5 and 6, for the 532 nm and
22 1064 nm channels, respectively. CALIOP-SODA derived using the 1L (CAL_S 1L) and 2L (CAL_S
23 2L) methods are depicted in black and blue, while CALIPSO V4 (CAL_{V4}) is in red. The main
24 differences, in agreement in AOD differences in Figure 4, are found: a) over IO and NEA where
25 CALIPSO V4 extinction profiles are higher than CALIOP-SODA, and b) over SEA, with lower
26 V4 extinctions than CALIOP-SODA. Even though the main V4-SODA differences in extinction
27 decrease during nighttime, especially over the SEA, the nighttime differences for NEA and IO
28 remain nearly the same. Interestingly, the higher CALIOP V4 extinction for NEA and IO
29 resembles the CALIPSO V4 overestimation during Caribbean 2010 (Fig. 3). CALIOP-SODA and
30 V4 profiles differences for regions with small AOD differences, such as the south Pacific (SP) and
31 the northwest Pacific (NWP), are modest. Another interesting aspect is the generally higher



1 variability of daytime CALIPSO V4 relative to SODA, manifested in the high standard deviations
2 in Figure 5 (error bars). This indicates that SODA retrievals are more stable than CALIPSO V4
3 especially during the daytime, due to the AOD constraint. Moreover, the high solar background
4 substantially degrades CALIPSO aerosol detection capabilities, affecting the retrieved extinction.
5 Lastly, CALIOP-SODA differences between 1L and 2L are small, and typically confined to a layer
6 below 700 m, where 2L tends to be smaller than 1L. This is explained, as in Section 4, by a
7 relatively shallow mixed-layer height (< 500 m), where $LR = 25$ sr for the 2L method.

8 For completeness, we show in Figure 6 the aerosol extinction profiles for the 1064 nm
9 channel. CALIOP-SODA and V4 profiles yield smaller differences relative to their 532 nm
10 counterpart, in agreement with ΔAOD (Figure 4).

11

12 **5.2. Maps of CALIOP-SODA Lidar ratio (LR) at 532 nm**

13 Figures 7 and 8 depict global maps of 532 nm LR derived from the 1L (LR_{1L}) and 2L
14 (LR_{2L}) assumptions, temporally averaged from March to August (MAMJJA, boreal spring-
15 summer) and September to February (SONDJF, boreal autumn-winter) of 2010 from the 25-km
16 averaged retrievals with cloud fraction less than 67%. Daytime 532 nm LR exhibits a clear spatial
17 pattern with high values (>45 sr) in coastal regions especially off the southwestern African coast
18 and east of China. The lowest values are observed over the western and central equatorial Pacific,
19 with ratios less than 30 sr, which are typical of clean maritime environments (e.g. Burton et al.,
20 2013). Semiannual transitions are primarily found near the continents, namely, the Southeast
21 Atlantic, Mediterranean Sea, Indian Ocean, and off the coast of eastern Asia. Nighttime LRs are
22 similar to their daytime counterparts, but with slightly higher values and a rather heterogeneous
23 pattern, likely attributed to the reduced cloud-free sampling at night due to the increased cloud
24 cover, especially over subtropical regions where stratiform and shallow cumulus clouds are
25 abundant.

26 Comparing the two layer assumptions, LR_{2L} (Figure 9) is higher than LR_{1L} , especially for
27 lidar ratios > 40 sr. This result is expected, as the prescribed MBL lidar ratio of 25 sr for 2L tends
28 to be lower than the lidar ratio for any aerosol type that would be found above the marine boundary
29 layer, and therefore lower than the column average or column effective lidar ratio. Therefore, to
30 match the SODA AOD, the lidar ratio above the MBL in the 2L case must be larger than the
31 column effective value that the 1L case derives. Overall, LR_{1L} and LR_{2L} differences are relatively



1 small (~ 5 sr), which, as we will show in the next section, is associated with the shallow MBL
2 height estimated from the bulk Richardson number method, and therefore a relatively small
3 fraction of aerosol that is controlled by the assumed marine lidar ratio in the 2L method.

4

5 **5.3. Fractional CALIOP-SODA AOD at 532 nm in the marine boundary layer**

6 CALIOP-SODA aerosol extinctions are further utilized for quantifying AOD in the
7 boundary layer. We first show in Figure 9 the 2010 semiannual total SODA AOD for daytime
8 (left) and nighttime (right) CALIPSO overpasses. Consistent with several studies (e.g. Kittaka et
9 al., 2011; Redemann et al., 2012), high AOD primarily occur over the eastern Atlantic, in
10 connection with biomass burning and dust emissions from southern and equatorial Africa. A
11 second region of interest encompasses most of the Asian coastal region, where a combination of
12 pollution and dust give rise to high AOD (Itahashi et al., 2010).

13 Before presenting MBL AOD, we show the MBL height maps (Figure 10), with typical
14 heights below 800 m, and littoral maxima up to 1150 m in northern Africa and Eurasia. Next, we
15 compute MBL AOD by numerically integrating CALIOP-SODA aerosol extinction coefficient
16 from the surface to the MBL height. MBL AOD in Figure 11 shows a dissimilar pattern relative
17 to its total AOD counterpart (Figure 9), manifested in a less dominant role of the southeast Atlantic.
18 In addition, coastal Africa, Eurasia, and North America exhibit peaks in MBL AOD (>0.12) during
19 boreal spring-summer. A second region with high AOD encompasses the extratropical oceans
20 poleward of 45° S/N, with a particularly consistent zonal band with high AOD in the Southern
21 Ocean. As expected, 2L MBL AOD is lower than 1L due to the 2L assumption of a lidar ratio =
22 25 sr in the MBL. Except for the subtropical ocean, which features shallow MBL and low MBL
23 AOD, a spatial modulation of the marine boundary layer in the MBL AOD is unclear. It is
24 important to mention that estimates of the AOD apportioned in the boundary layer will depend on
25 the MBL dataset utilized in the calculations. An alternative MBL height estimation derived from
26 CALIOP attenuated backscatter (McGrath-Sprangler and Denning, 2013) yields similar if not
27 slightly higher values than our GEOS-based MBL. However, MBL estimates based on
28 thermodynamical vertical profiles (temperature, relative humidity) from meteorological analyses
29 produce significantly higher MBL (von Engel and Teixeira, 2013), closely matching the cloud
30 top height of stratiform and shallow cumulus clouds. Thus, the MBL used here is expected to
31 primarily represents the mixed-layer height (von Engel and Teixeira, 2013).



1 The fraction of MBL AOD relative to the total is depicted in Fig. 12. The extratropical
2 bands show the highest fraction of MBL AOD, accounting for up to 0.73 (73%) of the total AOD.
3 Low fractions are found in the subtropics and tropics, with the lowest AOD fraction over the
4 eastern Atlantic and the west-central Pacific. Interestingly, vast areas over the ocean feature AOD
5 fractions of less than 40%, suggesting a significant contribution of free tropospheric aerosols to
6 the total AOD. These results are qualitatively consistent with the results Bourgeois et al. (2018)
7 using CALIPSO version 4.1.

8

9 **6. Discussion**

10 Due to the limited airborne and ground-based observations of lidar ratios over the ocean, a
11 global assessment of CALIOP-SODA retrievals is challenging. One of the few global satellite-
12 based estimates of lidar ratio is reported in Bréon (2013) who estimated LR utilizing the retrieved
13 scattering phase function at 180° angle derived from the Polarization and Directionality of the
14 Earth's Reflectances (POLDER) satellite instrument and a prescribed aerosol model. POLDER
15 LR is somewhat comparable to CALIOP-SODA (Figure 8-9) with both retrievals yielding high
16 LR over the coasts of eastern Africa and Eurasia, and a notable increase in LR over the Indian
17 Ocean in boreal autumn-winter. In addition, both POLDER and CALIOP-SODA produce LR < 30
18 sr over the open ocean. On the other hand, LR from POLDER tend to be slightly higher, with a
19 typical range between 30-70 sr. Bréon (2013) also indicates that because POLDER retrievals rely
20 on scattered photon measurements, LR might be biased low in regions dominated by absorbing
21 aerosol, such as the southeast Atlantic. A somewhat different method of retrieving LR from SODA
22 AOD, documented in Josset et al. (2011), consists of analytically solving the lidar equation. The
23 only available global analysis of LR using the technique in Josset et al. (2011) is documented in
24 Dawson et al. (2015) for maritime aerosols only, reporting values between 20-40 sr.

25 As different aerosol types can be, to some extent, characterized by their lidar ratio, the
26 reliability of CALIOP-SODA LR retrievals is qualitatively assessed by analyzing the consistency
27 between the CALIOP-SODA LR spatial pattern and the regional occurrence of aerosol types.
28 Burton et al. (2012), using HSRL measurements over North America and the adjacent Atlantic
29 Ocean, provide the following lidar ratios for a number of aerosol types: the highest LR (45-80 sr)
30 are typically attributed to smoke and urban aerosols, LR of 25-50 sr and 40 sr are associated with
31 dust and polluted maritime aerosols (respectively), and maritime aerosols are characterized by lidar



1 ratios of less than 30 sr. Following the classification of Burton et al. (2012), CALIOP SODA lidar
2 ratios (Fig. 7-8) will be interpreted in the context of major variations in atmospheric aerosols over
3 the global oceans. For simplicity, we will primarily interpret daytime LR_{1L} in Figures 7a and c.
4 Two distinct maxima in CALIOP-SODA LR ($LR > 50$ sr) for spring-summer (Figure 8a) are found
5 over the southeast Atlantic and the Mediterranean Sea. The LR peak in the southeast Atlantic is
6 explained by the well-documented biomass burning season over southern Africa, with massive
7 fires events from May to September during the dry season (Roberts et al., 2009), and smoke being
8 transported offshore by the prevailing winds during July to October (Adebisi et al., 2015). The high
9 spring-summer LR over the Mediterranean Sea is also expected given the southward pollution
10 transport from Europe which is maximized in summer (Duncan and Bey, 2004). A major LR
11 maximum in autumn-winter is observed south of India, over the Bay of Bengal and part of the
12 Arabian Sea. This pattern is concomitant with the pervasive presence of pollution and biomass
13 burning during the winter and pre-monsoon season (October to April, Krishnamurti et al., 2009).
14 In contrast, during the monsoon season (June-September), dust aerosols become the dominant
15 species over the Bay of Bengal (Das et al., 2013), which is manifested in the substantial reduction
16 in SODA LR in spring-summer. Regions with intermediate CALIOP-SODA LR ($35 \text{ sr} < LR < 50$
17 sr) are located over broad regions of the eastern Pacific, as well as narrow littoral bands over
18 eastern Asian and the east coast of North America. These regions are likely influenced by a
19 combination of maritime aerosols and pollution from the continents. Lastly, the regions with the
20 lowest LR are located over the tropical ocean, where AOD is the lowest (Figure 10). LR over the
21 Southern Ocean is typically around 30-35 sr, which is rather surprising for such a remote region
22 with limited continental influence, where maritime aerosols (and associated lidar ratios near 25 sr)
23 are expected to be the dominant aerosol type. Interestingly, Omar et al. (2009) noted a large
24 number of cases in which the CALIPSO aerosol classification algorithm detected continental clean
25 aerosol, which in turn, the CALIPSO algorithm assigns a 532 nm lidar ratio of 35 sr (version 3)
26 and 53 sr (version 4.1). Lastly, the interpretation the 1064 nm CALIOP-SODA is not attempted
27 here due to the lack of independent measurements and calibration uncertainties associated with the
28 use of CALIPSO V3 for deriving SODA AOD. A future release of SODA based on CALIPSO V4
29 will benefit from the improved calibration of V4, which is estimated to be within 3% (Vaughan et
30 al., 2018).



1 An aspect that deserves further discussion is the reliability of SODA AOD, as it is essential
2 for constraining the lidar equation in our study. In this study we find a high linear correlation
3 between SODA and HSRL AOD ($r=0.96$), with no clear relationship between SODA biases and
4 AOD magnitudes, and a SODA-to-HSRL RSME comparable to the one estimated between SODA
5 and AERONET in Dawson et al. (2015). The differences between SODA and the CALIPSO V4
6 AOD (Figure 4) also support inferences based on comparisons between MODIS and CALIPSO
7 Science Team AOD over the ocean (Redemann et al., 2012; Kim et al., 2013). Analogous to our
8 results, Redemann et al. (2012) found an underestimation of CALIOP Version 3 of MODIS
9 collection 5 over the southeast Atlantic in July, and overestimation over the Bay of Bengal and the
10 zonal band near the equatorial Atlantic Ocean. Redemann et al. (2012) and our results both point
11 to an overestimation of CALIPSO V4 AOD over oceanic regions dominated by dust, and
12 underestimation in regions dominated by smoke. To verify that SODA-CALIPSO V4 differences
13 are mainly attributed to CALIPSO V4 biases, we perform an additional comparison using Aqua-
14 MODIS Level 2 550 nm AOD (MYD04_3K product), taken from the latest Collection 6.1 (Levy
15 et al., 2013) for the June to September period of 2010. Cloud-free 3-km MODIS AOD pixels are
16 collocated with CALIPSO track and averaged to approximately 25 km (along track) to match the
17 averaged 25 km SODA retrievals. Next, MODIS-SODA mean differences are averaged every
18 $6^\circ \times 3^\circ$ grid, and depicted in Figure 13. The MODIS-SODA differences in Figure 13 are typically
19 within the $[0.06 -0.06]$ range, with negligible values over the eastern Atlantic and the northwest
20 Pacific. Although Δ AOD reaches up to 0.12 over the Indian Ocean, these differences are smaller
21 than those between CALIPSO V4 and SODA (Figure 4, upper left panel). Overall, MODIS further
22 corroborates that CALIPSO V4 AOD is biased over regions dominated by smoke and dust. We
23 note that the plausible oceanic CALIOP V4 bias dependence on aerosol types suggested in our
24 study might not be applicable over land, where AOD for dust is underestimated by CALIPSO (e.g.
25 Schuster et al., 2012).

26

27 **7. Concluding remarks**

28 One year of a new CALIOP-based aerosol extinction coefficient and lidar ratio dataset has
29 been presented, with the goal of providing a flexible dataset for climate research as well as
30 independent retrievals that can be helpful for refining CALIPSO Science Team algorithms. The
31 new retrievals build on the CALIPSO V4 total attenuated backscatter and cloud mask data



1 products. However, the method that we used to invert the lidar equation differs fundamentally from
2 the CALIOP standard aerosol product, as it does not rely upon an aerosol classification module to
3 prescribe the lidar ratio. We evaluated CALIOP-SODA AOD, LR, and extinction using airborne
4 HSRL retrievals over the western Atlantic, and found excellent agreement, with statistically
5 significant correlations and biases less than 27 %. Given these encouraging results, we envision
6 potential uses of CALIOP-SODA lidar ratios for evaluating CALIOP V4 aerosol properties. This
7 can be done similar to Dawson et al. (2015), by stratifying CALIOP-SODA LR as a function of
8 CALIOP V4 aerosol types and their assigned lidar ratio.

9 Although the retrievals presented here are limited to cloud-free atmospheric columns due
10 to the constraint imposed by SODA AOD, it is possible to adapt the algorithm to make use of
11 above-cloud satellite AOD retrievals (e.g., Jethva et al., 2014; Liu et al., 2015). In this regard,
12 above-cloud AOD using CALIOP can be derived by combining the integrated attenuated
13 backscatter and depolarization ratio (Hu et al., 2007; Liu et al., 2015), with corrections for the
14 multiple-scattering depolarization relationship implemented by SODA (Deaconu et al., 2017).
15 Efforts to retrieve above-cloud lidar ratio and extinction profiles over the southeast Atlantic using
16 the above cloud AOD are currently underway (Ferrare et al., 2018).

17 CALIOP-SODA 1L retrievals are expected to perform better for relatively homogeneous
18 atmospheric profiles characterized by a single aerosol type. Alternatively, SODA 2L retrievals are
19 likely to be advantageous for specific regions where massive aerosol plumes from the continent
20 are transported offshore at high altitudes through convective processes, in such a way that MBL
21 aerosols are detached from the layer above and the assumption MBL LR=25 sr (maritime) is a
22 good approximation. This is probably the case over the southeast Atlantic during the biomass
23 burning season or for episodic dust transport over the tropical Atlantic. However, the CALIPSO
24 Science Team product will continue providing the best available global dataset for monitoring
25 complex aerosol profiles, continental processes, and aerosols in the upper troposphere.

26

27 *Data availability.* CALIPSO version 4.1 is available at <https://eosweb.larc.nasa.gov>, and SODA
28 aerosol optical depth at <http://www.icare.univ-lille1.fr>.

29 *Competing interests.* The authors declare that they have no conflict of interest.

30



1 *Acknowledgements: This work was funded by the CloudSat and CALIPSO Science Reconnect*
2 *Program NASA award # NNH16CY04C. The SODA product is developed at the AERIS/ICARE*
3 *data and services center (<http://www.icare.univ-lille1.fr/projects/soda>) in Lille (France) in the*
4 *frame of the CALIPSO mission and supported by CNES. The AERIS data infrastructure is greatly*
5 *acknowledged for data, processing and development supports of the SODA product. We thank Dr.*
6 *Gregory Schuster for his insightful comments and suggestions.*
7

8

9 **References**

10 Adebisi, A.A., Zuidema, P., and Abel, S.J.: The Convolution of Dynamics and Moisture
11 with the Presence of Shortwave Absorbing Aerosols over the Southeast Atlantic, *J.*
12 *Climate*, **28**, 1997–2024, <https://doi.org/10.1175/JCLI-D-14-00352.1>, 2015.

13 Bourgeois, Q., Ekman, A. M. L., Renard, J.-B., Krejci, R., Devasthale, A., Bender, F., et
14 al.: How much of the global aerosol optical depth is found in the boundary layer and free
15 troposphere?, *Atmos. Chem. Phys.*, **18**, 7709–7720, 2018.

16 Bréon, F.-M.: Aerosol extinction-to-backscatter ratio derived from passive satellite
17 measurements, *Atmos. Chem. Phys.*, **13**, 8947–8954, <https://doi.org/10.5194/acp-13-8947-2013>,
18 2013.

19 Burton, S. P., et al.: Using airborne high spectral resolution lidar data to evaluate combined
20 active plus passive retrievals of aerosol extinction profiles, *J. Geophys. Res.*, **115**, D00H15,
21 doi: 10.1029/2009JD012130, 2010.

22 Burton, S. P., Ferrare, R. A., Hostetler, C. A., Hair, J. W., Rogers, R. R., Obland, M. D., et
23 al.: Aerosol classification using airborne High Spectral Resolution Lidar measurements –
24 methodology and examples, *Atmos. Meas. Tech.*, **5**, 73–98, <https://doi.org/10.5194/amt-5-73-2012>,
25 2012.

26 Burton, S. P., Ferrare, R. A., Vaughan, M. A., Omar, A. H., Rogers, R. R., Hostetler, C.
27 A., and Hair, J. W.: Aerosol classification from airborne HSRL and comparisons with the
28 CALIPSO vertical feature mask, *Atmos. Meas. Tech.*, **6**, 1397–1412, [https://doi.org/10.5194/amt-](https://doi.org/10.5194/amt-6-1397-2013)
29 [6-1397-2013](https://doi.org/10.5194/amt-6-1397-2013), 2013.

30 Das, S., Dey, S., Dash, S. K., and Basil, G.: Examining mineral dust transport over the
31 Indian subcontinent using the regional climate model, RegCM4.1, *Atmos. Res.*, **134**, 64–76, 2013

32 Das, S., H. Harshvardhan, H. Bian, M. Chin, G. Curci, A. P. Protonotariou, T.
33 Mielonen, K. Zhang, H. Wang, and X. Liu: Biomass burning aerosol transport and vertical



- 1 distribution over the South African-Atlantic region, *J. Geophys. Res. Atmos.*, 122, 6391–6415,
2 doi: 10.1002/2016JD026421, 2017.
- 3 Dawson, K. W., Meskhidze, N., Josset, D., and Gassó, S.: Spaceborne observations of the
4 lidar ratio of marine aerosols, *Atmos. Chem. Phys.*, 15, 3241–3255, [https://doi.org/10.5194/acp-15-](https://doi.org/10.5194/acp-15-3241-2015)
5 3241-2015, 2015.
- 6 Deaconu, L. T., Waquet, F., Josset, D., Ferlay, N., Peers, F., Thieuleux, F., Ducos, F.,
7 Pascal, N., Tanré, D., Pelon, J., and Goloub, P.: Consistency of aerosols above clouds
8 characterization from A-Train active and passive measurements, *Atmos. Meas. Tech.*, 10, 3499-
9 3523, <https://doi.org/10.5194/amt-10-3499-2017>, 2017.
- 10 de Laat, A. T. J., Stein Zweers, D. C. , Boers, R., and Tuinder, O. N. E.: A solar escalator:
11 Observational evidence of the self-lifting of smoke and aerosols by absorption of solar radiation
12 in the February 2009 Australian Black Saturday plume, *J. Geophys. Res.*, 117, D04204,
13 doi:10.1029/2011JD017016, 2012.
- 14 Duncan, B. N. and Bey, I.: A modeling study of the export pathways of pollution from
15 Europe: Seasonal and interannual variations (1987–1997), *J. Geophys. Res.*, 109, D08301,
16 doi:10.1029/2003JD004079, 2004.
- 17 Eloranta, E. W.: High spectral resolution lidar, in *Lidar. Range- Resolved Optical Remote*
18 *Sensing of the Atmosphere*, edited by C. Weitkamp, pp. 143–163, Springer, New York, 2005.
- 19 Fernald, F. G.: Analysis of atmospheric lidar observations: Some comments, *Appl. Opt.*, 23,
20 652–653, doi:10.1364/AO.23.000652, 1984.
- 21 Ferrare R., Burton, S., Cook A. L., Harper, D. B., Hostetler, C., Hair, J., et al. CALIOP and
22 Airborne HSRL-2 Measurements of Smoke above low clouds during ORACLES.
23 CloudSat/CALIPSO Annual Science Review, 23-25 April 2018, Boulder Colorado, USA., 2018.
- 24 Gravseth, I. J. and Piepe, B.: CloudSat’s return to the A-Train, *International Journal of*
25 *Space Science and Engineering*, 1, 410–431, doi:10.1504/IJSPACESE.2013.059269, 2013.
- 26 Hair, J. W., Hostetler, C. A., Cook, A. L., Harper, D. B., Ferrare, R. A., Mack, T. L.,
27 Welch, W., Izquierdo, L. R., and Hovis, F. E.: Airborne high spectral resolution lidar for pro-
28 filing aerosol optical properties, *Appl. Optics*, 47, 6734–6752, doi:10.1364/AO.47.006734, 2008.
- 29 Hu, Y., Vaughan, M., Liu, Z., Powell, K., and Rodier, S.: Retrieving optical depths and
30 lidar ratios for transparent layers above opaque water clouds from CALIPSO lidar



- 1 measurements, *IEEE Geosci. Remote Sens. Lett.*, **4**(4), 523–526, doi:10.1109/LGRS.2007.901085,
2 2007.
- 3 Itahashi, S., K. Yumimoto, I. Uno, K. Eguchi, T. Takemura, Y. Hara, A. Shimizu, N.
4 Sugimoto, and Liu, Z.: Structure of dust and air pollutant outflow over East Asia in the
5 spring, *Geophys. Res. Lett.*, **37**, L20806, doi: 10.1029/2010GL044776, 2010.
- 6 Jethva, H., Torres, O., Waquet, F., Chand, D., and Hu, Y.: How do A-train sensors
7 intercompare in the retrieval of above-cloud aerosol optical depth? A case study-based
8 assessment, *Geophys. Res. Lett.*, **41**, 186–192, doi: 10.1002/2013GL058405, 2014.
- 9 Josset, D., Pelon, J., Protat, A., and Flamant, C.: New approach to determine aerosol
10 optical depth from combined CALIPSO and CloudSat ocean surface echoes, *Geophys. Res.
11 Lett.*, **35**, L10805, doi: 10.1029/2008GL033442, 2008.
- 12 Josset, D., Pelon, J., and Hu, Y.: Multi-instrument calibration method based on a
13 multiwavelength ocean surface model, *IEEE Geosci. Remote Sens. Lett.*, **7**, 195–199, doi:
14 10.1109/LGRS.2009.2030906, 2010.
- 15 Josset D., Rogers, R., Pelon, J., Hu, Y., Liu, Z., Omar, A., et al.: CALIPSO lidar ratio
16 retrieval over the ocean, *Opt. Express*, **19**, 18696-18706, 2011.
- 17 Josset, D., Tanelli, S., Hu, Y., Pelon, J., Zhai, P.: Analysis of water vapor correction for
18 CloudSat W-band radar", *IEEE Trans. Geosci. Remote Sens.*, vol. 51, no. 7, pp. 3812-3825, 2013.
- 19 Josset, D., Hou, W., Pelon, J., Hu, Y., Tanelli, S., Ferrare, R., et al.: Ocean and polarization
20 observations from active remote sensing: atmospheric and ocean science applications. *Proc. SPIE
21 9459, Ocean Sensing and Monitoring VII*, 94590N, doi:10.1117/12.2181544, 2015.
- 22 Khaykin, S. M., Godin-Beekmann, S., Hauchecorne, A., Pelon, J., Ravetta, F., and
23 Keckhut, P.: Stratospheric smoke with unprecedentedly high backscatter observed by lidars above
24 southern France, *Geophys. Res. Lett.*, **45**, 1639–1646, doi:10.1002/2017GL076763, 2018.
- 25 Kim, M.-H., Kim, S.-W., Yoon, S.-C., and Omar, A. H.: Comparison of aerosol optical
26 depth between CALIOP and MODIS-Aqua for CALIOP aerosol subtypes over the ocean, *J.
27 Geophys. Res. Atmos.*, **118**, 13,241–13,252, doi: 10.1002/2013JD019527, 2013.
- 28 Kim, M.-H., Omar, A. H., Tackett, J. L., Vaughan, M. A., Winker, D. M., Trepte, C. R.,
29 Hu, Y., Liu, Z., Poole, L. R., Pitts, M. C., Kar, J., and Magill, B. E.: The CALIPSO Version 4
30 Automated Aerosol Classification and Lidar Ratio Selection Algorithm, *Atmos. Meas. Tech.
31 Discuss.*, <https://doi.org/10.5194/amt-2018-166>, in review, 2018.



- 1 Kittaka, C., Winker, D. M., Vaughan, M. A., Omar, A., and Remer, L. A.: Intercomparison
2 of column aerosol optical depths from CALIPSO and MODIS-Aqua, *Atmos. Meas. Tech.*, 4, 131-
3 141, <https://doi.org/10.5194/amt-4-131-2011>, 2011.
- 4 Koffi, B., et al.: Evaluation of the aerosol vertical distribution in global aerosol models
5 through comparison against CALIOP measurements: AeroCom phase II results, *J. Geophys. Res.*
6 *Atmos.*, 121, 7254–7283, doi: 10.1002/2015JD024639, 2016.
- 7 Krishnamurti, T. N., Chakraborty, A., Martin, A., Lau, W. K., Kim, K.-M., Sud, Y., and
8 Walker, G.: Impact of Arabian Sea pollution on the Bay of Bengal winter monsoon rains, *J.*
9 *Geophys. Res.*, 114, D06213, doi: 10.1029/2008JD010679, 2009.
- 10 Levy, R. C., Mattoo, S., Munchak, L. A., Remer, L. A., Sayer, A. M., Patadia, F., and Hsu,
11 N. C.: The Collection 6 MODIS aerosol products over land and ocean, *Atmos. Meas. Tech.*, 6,
12 2989-3034, <https://doi.org/10.5194/amt-6-2989-2013>, 2013.
- 13 Liu, Z., Omar, A., Vaughan, M., Hair, J., Kittaka, C., Hu, Y., Powell, K., Treppe, C.,
14 Winker, D., Hostetler, C., Ferrare, R., and Pierce, R.: CALIPSO lidar observations of the optical
15 properties of Saharan dust: A case study of long-range transport, *J. Geophys. Res.*, 113, D07207,
16 doi: 10.1029/2007JD008878, 2008.
- 17 Liu, Z., Winker, D., Omar, A., Vaughan, M., Kar, J., Treppe, C., Hu, Y., and Schuster, G.:
18 Evaluation of CALIOP 532 nm aerosol optical depth over opaque water clouds, *Atmos. Chem.*
19 *Phys.*, 15, 1265-1288, <https://doi.org/10.5194/acp-15-1265-2015>, 2015.
- 20 McGrath-Spangler, E. L., and Denning, A. S.: Global seasonal variations of midday
21 planetary boundary layer depth from CALIPSO space-borne LIDAR, *J. Geophys. Res.*
22 *Atmos.*, 118, 1226–1233, doi: 10.1002/jgrd.50198, 2013.
- 23 McGrath-Spangler, E. L. and Molod, A.: Comparison of GEOS-5 AGCM planetary
24 boundary layer depths computed with various definitions. *Atmos. Chem. Phys.*, 14, 6717-6727,
25 <https://doi.org/10.5194/acp-14-6717-2014>, 2014.
- 26 Müller, D., Ansmann, A., Mattis, I., Tesche, M., Wandinger, U., Althausen, D., and Pisani,
27 G.: Aerosol-type-dependent lidar ratios observed with Raman lidar, *J. Geophys. Res.*, 112,
28 D16202, doi: 10.1029/2006JD008292, 2007.
- 29 Nowottnick, E. P., Colarco, P. R., Welton, E. J., and da Silva, A.: Use of the CALIOP
30 vertical feature mask for evaluating global aerosol models, *Atmos. Meas. Tech.*, 8, 3647-3669,
31 <https://doi.org/10.5194/amt-8-3647-2015>, 2015.



- 1 Redemann, J., Vaughan, M. A., Zhang, Q., Shinozuka, Y., Russell, P. B., Livingston, J.
2 M., Kacenelenbogen, M., and Remer, L. A.: The comparison of MODIS-Aqua (C5) and CALIOP
3 (V2 & V3) aerosol optical depth, *Atmos. Chem. Phys.*, 12, 3025-3043,
4 <https://doi.org/10.5194/acp-12-3025-2012>, 2012.
- 5 Roberts, G., Wooster, M. J., and Lagoudakis, E.: Annual and diurnal african biomass
6 burning temporal dynamics, *Biogeosciences*, 6, 849-866, <https://doi.org/10.5194/bg-6-849-2009>,
7 2009.
- 8 Rogers, R. R., Vaughan, M. A., Hostetler, C. A., Burton, S. P., Ferrare, R. A., Young, S.
9 A., Hair, J. W., Obland, M. D., Harper, D. B., Cook, A. L., and Winker, D. M.: Looking through
10 the haze: evaluating the CALIPSO level 2 aerosol optical depth using airborne high spectral
11 resolution lidar data, *Atmos. Meas. Tech.*, 7, 4317-4340, <https://doi.org/10.5194/amt-7-4317-2014>,
12 2014.
- 13 Royer, P., Raut, J.-C., Ajello, G., Berthier, S., and Chazette, P.: Synergy between CALIOP
14 and MODIS instruments for aerosol monitoring: application to the Po Valley, *Atmos. Meas. Tech.*,
15 3, 893-907, <https://doi.org/10.5194/amt-3-893-2010>, 2010.
- 16 Schuster, G. L., Vaughan, M., MacDonnell, D., Su, W., Winker, D., Dubovik, O.,
17 Lapyonok, T., and Trepte, C.: Comparison of CALIPSO aerosol optical depth retrievals to
18 AERONET measurements, and a climatology for the lidar ratio of dust, *Atmos. Chem. Phys.*, 12,
19 7431-7452, <https://doi.org/10.5194/acp-12-7431-2012>, 2012.
- 20 Thorsen, T. J., Ferrare, R. A., Hostetler, C. A., Vaughan, M. A., and Fu, Q.: The impact of
21 lidar detection sensitivity on assessing aerosol direct radiative effects, *Geophys. Res. Lett.*, 44,
22 9059–9067, doi:10.1002/2017GL074521, 2017.
- 23 Toth, T. D., Campbell, J. R., Reid, J. S., Tackett, J. L., Vaughan, M. A., Zhang, J., and
24 Marquis, J. W.: Minimum aerosol layer detection sensitivities and their subsequent impacts on
25 aerosol optical thickness retrievals in CALIPSO level 2 data products, *Atmos. Meas. Tech.*, 11,
26 499-514, <https://doi.org/10.5194/amt-11-499-2018>, 2018.
- 27 Uno, I., Eguchi, K., Yumimoto, K., Liu, Z., Hara, Y., Sugimoto, N., Shimizu, A., and
28 Takemura, T.: Large Asian dust layers continuously reached North America in April 2010, *Atmos.*
29 *Chem. Phys.*, 11, 7333-7341, <https://doi.org/10.5194/acp-11-7333-2011>, 2011.
- 30 Vaughan, M., Winker, D. M., and Powell, K. A.: CALIOP algorithm theoretical basis
31 document, Part 2: Feature detection and layer properties algorithms. NASA Langley Research



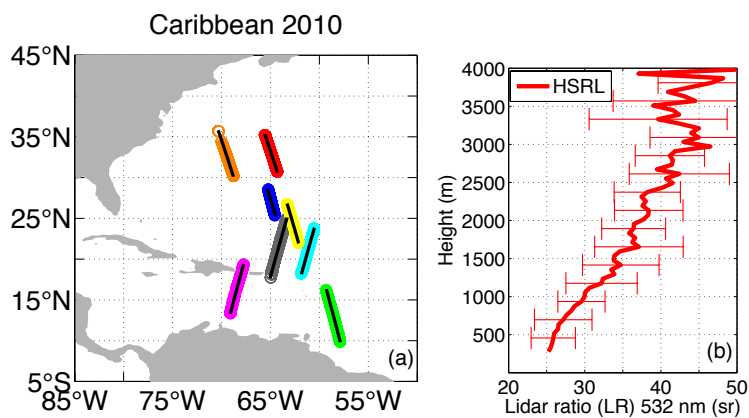
- 1 Center Document PC-SCI-202 Part 2, 87 pp. [Available online at [http://www-](http://www-calipso.larc.nasa.gov/resources/pdfs/PC-SCI_202_Part2_rev1x01.pdf)
2 [calipso.larc.nasa.gov/resources/pdfs/PC-SCI_202_Part2_rev1x01.pdf](http://www-calipso.larc.nasa.gov/resources/pdfs/PC-SCI_202_Part2_rev1x01.pdf)], 2005.
- 3 von Engel, A., and Teixeira, J.: A Planetary Boundary Layer Height Climatology Derived
4 from ECMWF Reanalysis Data. *J. Climate*, **26**, 6575–6590, <https://doi.org/10.1175/JCLI-D-12->
5 [00385.1](https://doi.org/10.1175/JCLI-D-12-00385.1), 2013.
- 6 Winker, D.M., Vaughan, M.A., Omar, A., Hu, Y., Powell, K.A., Liu, Z., et al.: Overview
7 of the CALIPSO Mission and CALIOP Data Processing Algorithms, *J. Atmos. Oceanic*
8 *Technol.*, **26**, 2310–2323, <https://doi.org/10.1175/2009JTECHA1281.1>, 2009.
- 9 Winker, D. M., and et al.: The CALIPSO Mission: A global 3D view of aerosols and
10 clouds, *Bull. Am. Meteorol. Soc.*, **91**, 1211–1229, doi:10.1175/2010BAMS3009.1, 2010.
- 11 Winker, D. M., Tackett, J. L., Getzewich, B. J., Liu, Z., Vaughan, M. A., and Rogers, R.
12 R.: The global 3-D distribution of tropospheric aerosols as characterized by CALIOP, *Atmos.*
13 *Chem. Phys.*, **13**, 3345–3361, <https://doi.org/10.5194/acp-13-3345-2013>, 2013.
- 14 Yu, H., Chin, M., Winker, D. M., Omar, A. H., Liu, Z., Kittaka, C., and Diehl, T.: Global
15 view of aerosol vertical distributions from CALIPSO lidar measurements and GOCART
16 simulations: Regional and seasonal variations, *J. Geophys. Res.*, **115**, D00H30,
17 doi:10.1029/2009JD013364, 2010.
- 18 Yu, H., Chin, M., Yuan, T., Bian, H., Remer, L. A., Prospero, J. M., Omar, A., Winker, D.,
19 Yang, Y., Zhang, Y., Zhang, Z., and Zhao, C.: The Fertilizing Role of African Dust in the Amazon
20 Rainforest: A First Multiyear Assessment Based on CALIPSO Lidar Observations, *Geophys. Res.*
21 *Lett.*, **42**, 1984–1991, doi:10.1002/2015GL063040., 2015.
- 22
23
24
25
26
27
28
29
30
31



1 **Figures**

2

3



4

5 Figure 1: a) Flight tracks during the 2010 field campaign. Black solid lines correspond to the

6 matched CALIPSO tracks. b) Mean HSRL lidar ratio (532 nm) as a function of altitude and one

7 standard deviation (error bar) for all the flight tracks in Fig. 1a.

8

9

10

11

12

13

14

15

16

17

18

19

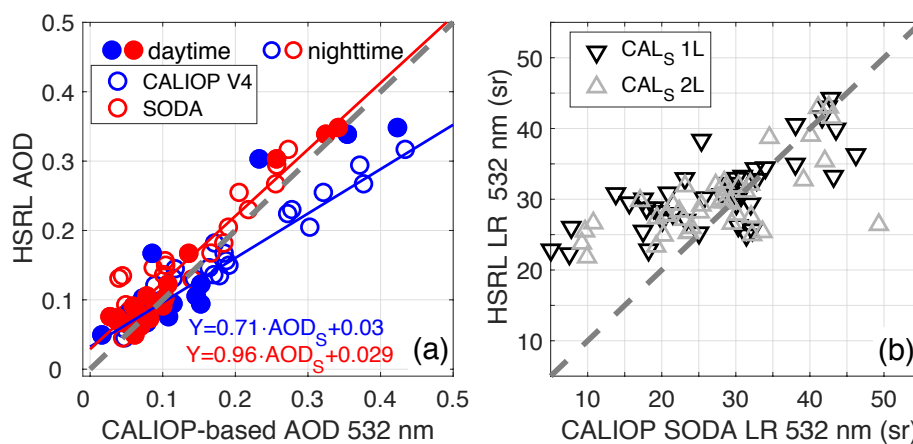
20

21

22



1



2

3 Figure 2: a) Scatterplot between SODA (red) and CALIPSO V4 (blue) against HSRL AOD at
 4 532 nm. Filled and open circles indicate daytime and nighttime observations, respectively. Blue
 5 and red lines (and equations) are the linear fit for V4 and SODA AOD (AOD_{V4} and AOD_S)
 6 relative to HSRL. b) Comparison between CALIPSO SODA (CAL_S) lidar ratio based on the 1-
 7 layer (1L) and 2-layer (2L) assumption with the HSRL column-effective lidar ratio from Eq. 4
 8 (black and gray symbols, respectively). Gray dashed line is the one-to-one relationship.

9

10

11

12

13

14

15

16

17

18

19

20

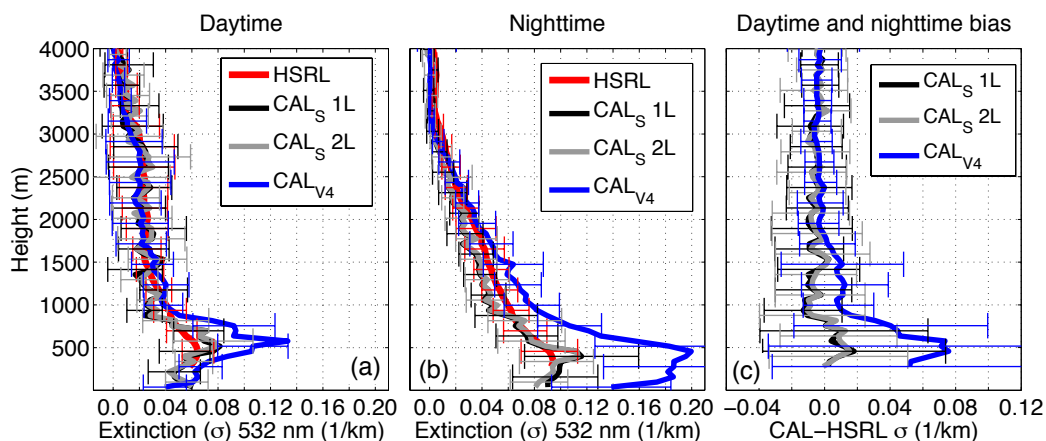
21

22

23



1



2

3 Figure 3: Mean aerosol extinction coefficient profile from the HSRL (red), CALIPSO SODA 1L
 4 (black), 2L (gray), and CALIPSO standard V4 product (blue) during a) daytime and b)
 5 nighttime. c) Total mean bias of CALIPSO-based extinction relative to the HSRL: CALIPSO
 6 SODA 1L (black) and 2L (gray), CALIPSO V4 (blue). Error bars in Fig. 3 a and b denote one
 7 standard deviation, and RMSE in Fig. 3c.

8

9

10

11

12

13

14

15

16

17

18

19

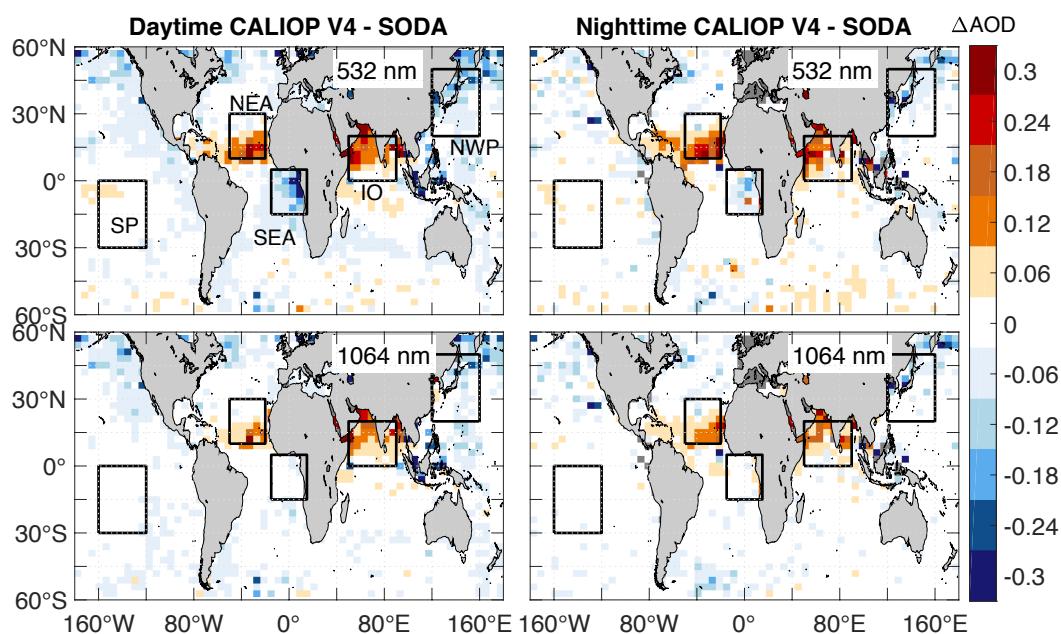
20

21

22



1



2

3 Figure 4: Mean AOD difference between CALIOP V4 and SODA for five months of 2010 for
 4 daytime (left) and nighttime (right), and the 532 nm (upper panels) and 1064 nm (lower panels)
 5 channels. Boxes denote specific regions in which the extinction coefficient profiles are further
 6 compared in Figure 5: South Pacific (SP), southeast Atlantic (SEA), Indian Ocean (IO), northeast
 7 Atlantic (NEA), and northwest Pacific (NWP).

8

9

10

11

12

13

14

15

16

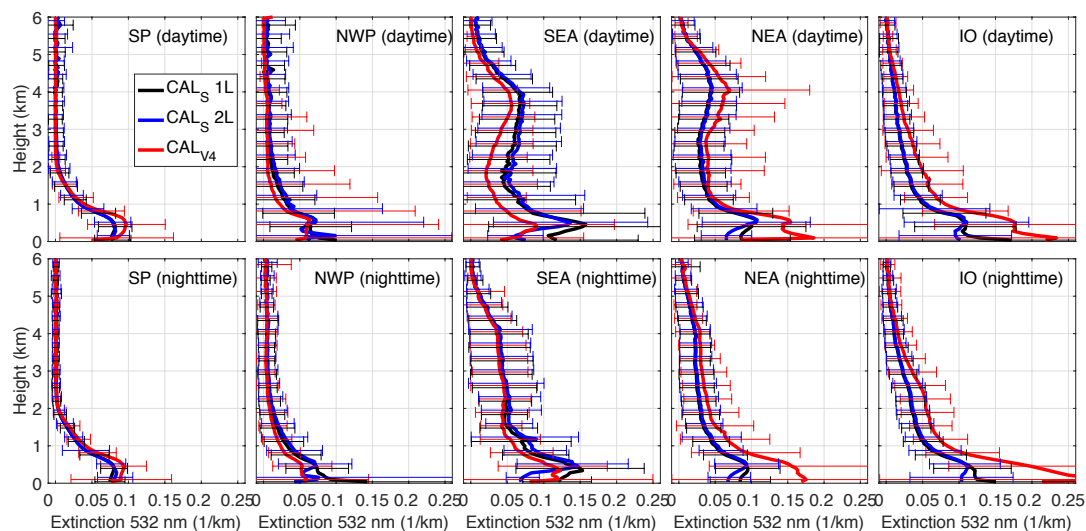
17

18

19



1



2

3

Figure 5: Mean aerosol extinction coefficient at 532 nm for the five regions defined in Fig. 4.

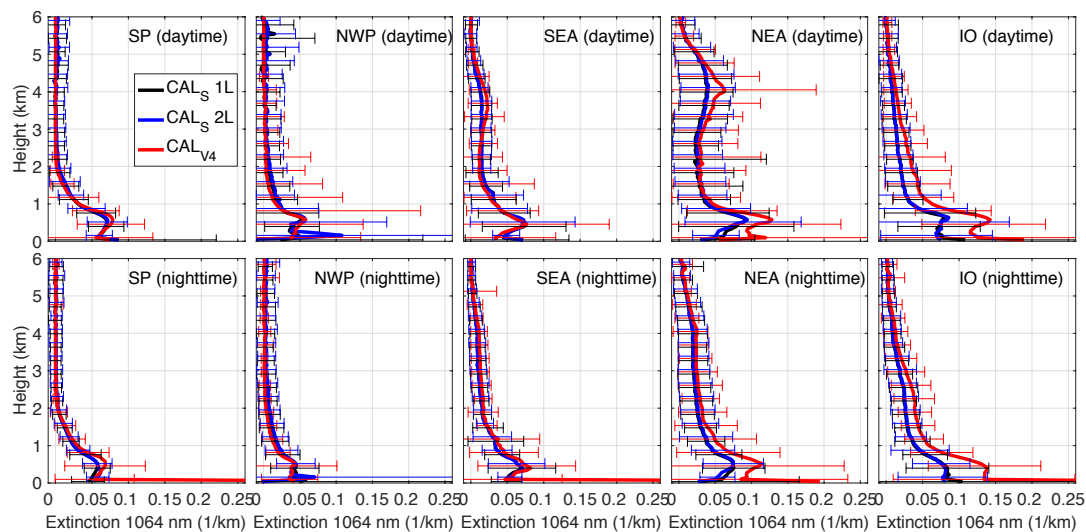
4

Upper and lower panels correspond to daytime and nighttime retrievals. CALIPSO-SODA

5

profiles are in black (1L) and blue (2L), and CALIPSO V4 is in red.

6



7

8

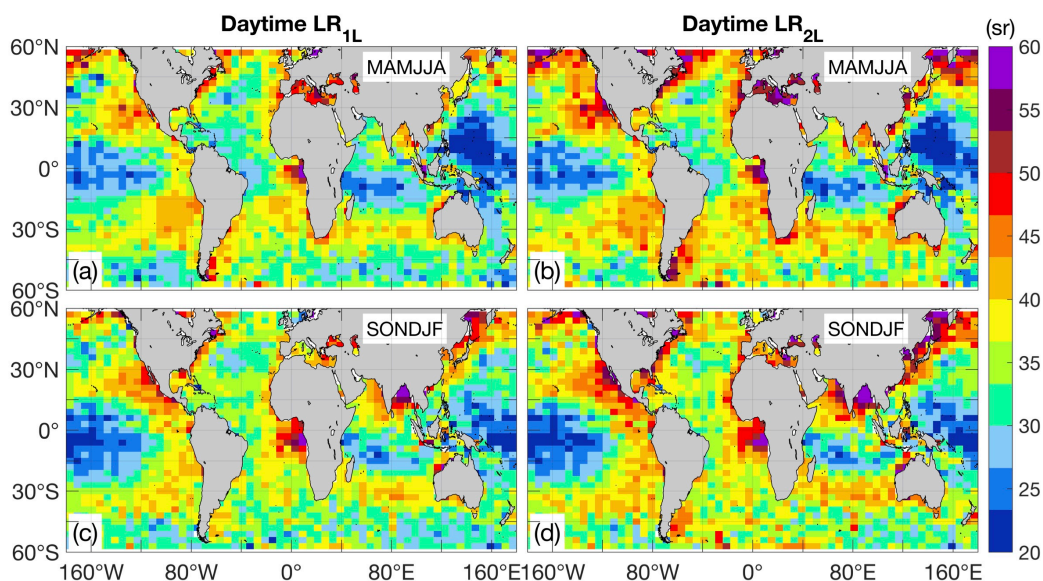
Figure 6: As in Figure 5 but for the 1064 nm channel.

9

10



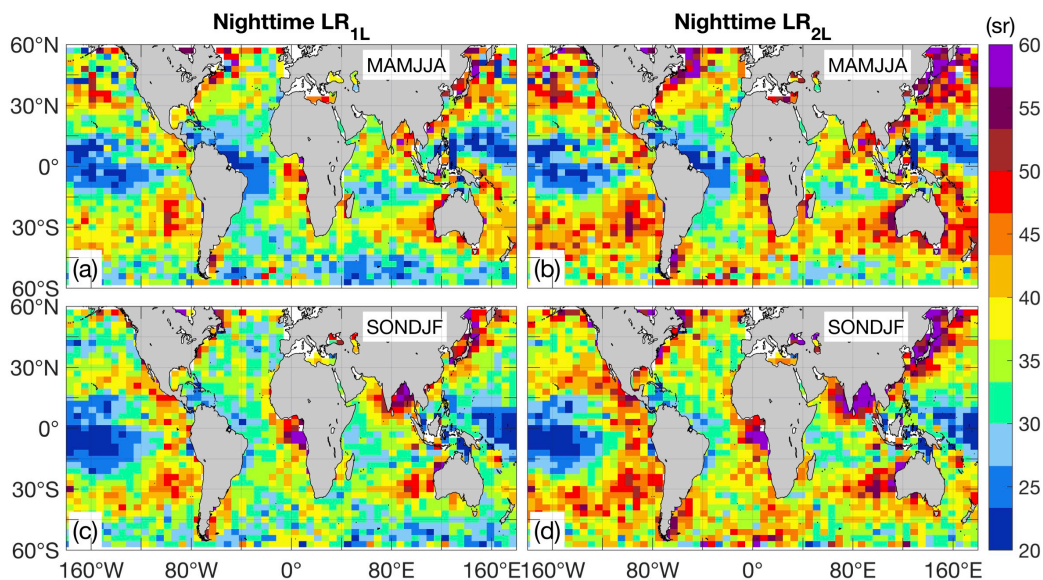
1



2

3 Figure 7: Semi-annual daytime 532 nm lidar ratios. a) LR_{1L} for spring-summer, b) LR_{2L} for
4 spring-summer, c) LR_{1L} for autumn-winter, and d) LR_{2L} for autumn-winter.

5



6

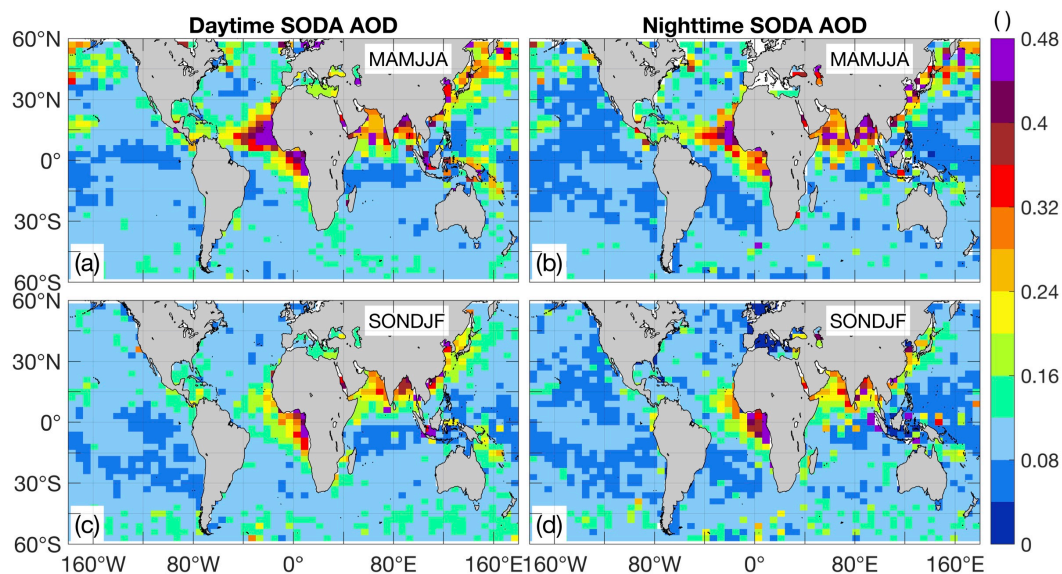
7

Figure 8: As in Figure 7 but for nighttime.



1

2

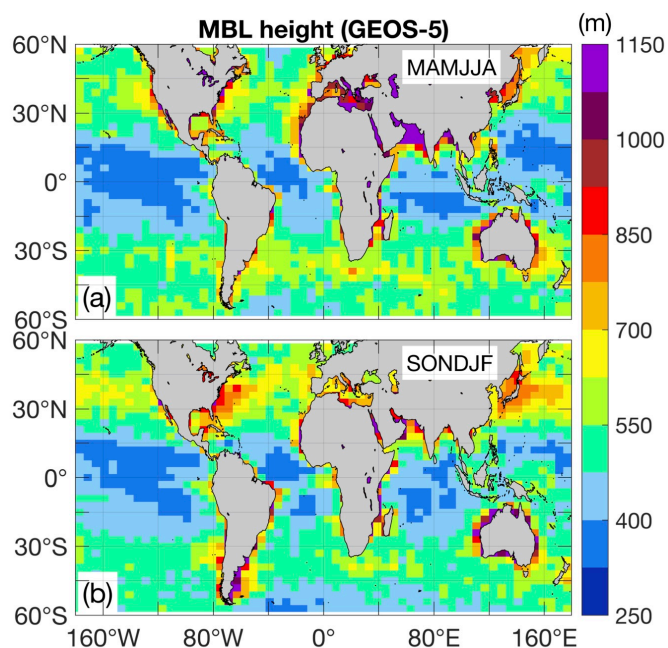


3

4 Figure 9: SODA AOD for daytime (a and c) and nighttime (b and d), spring-summer (MAMJJA)
5 and autumn-winter (SONDJF).
6
7
8
9
10
11
12
13
14
15
16
17
18
19



1



2

3

Figure 10: Daytime marine boundary layer height for a) spring-summer, and b) autumn-winter.

4

5

6

7

8

9

10

11

12

13

14

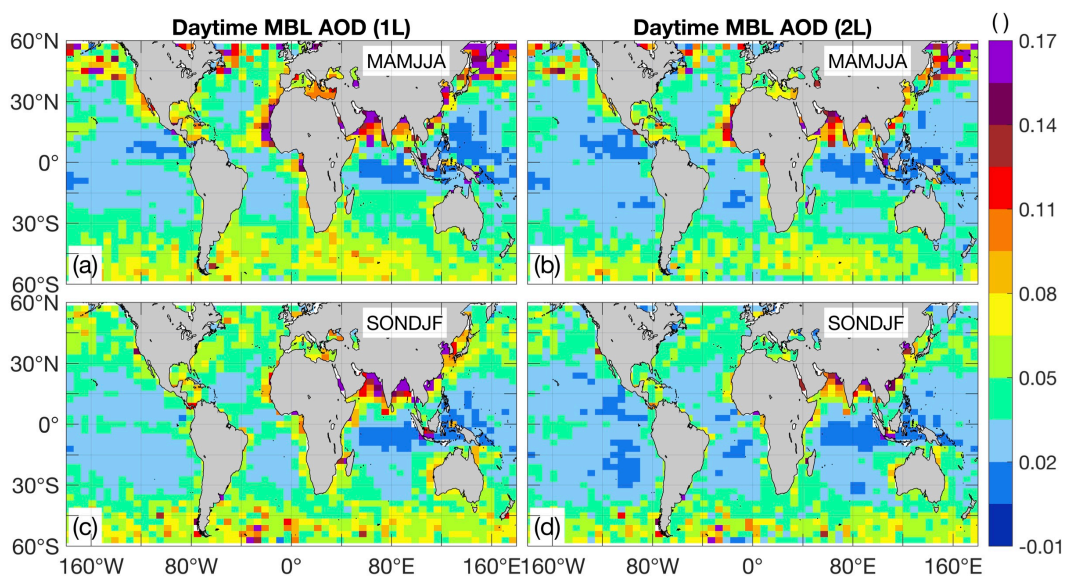
15

16

17



1



2

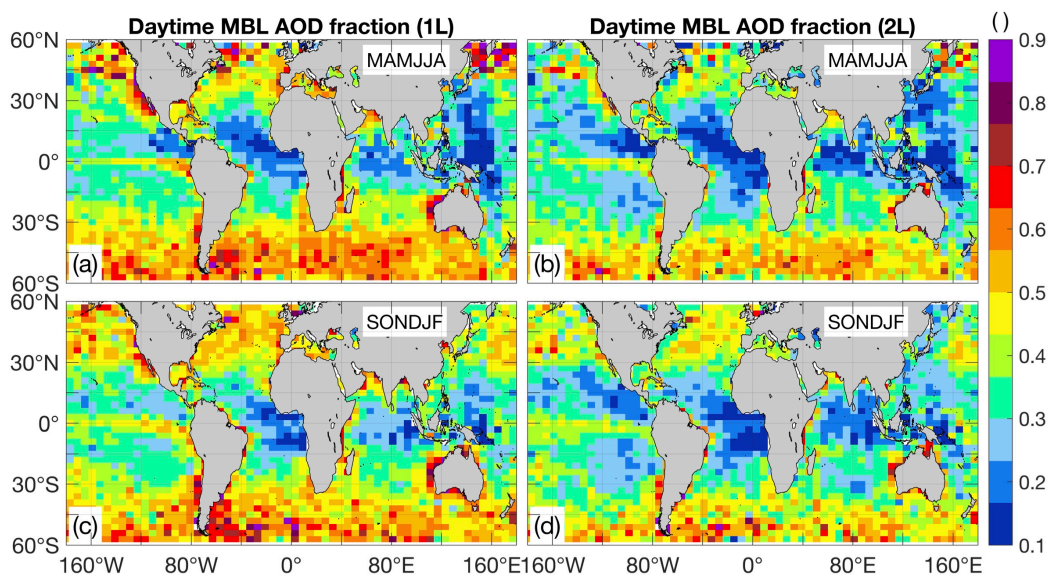
3

4

5

6

Figure 11: Daytime MBL 532 nm AOD based on 1L (left) and 2L (right).

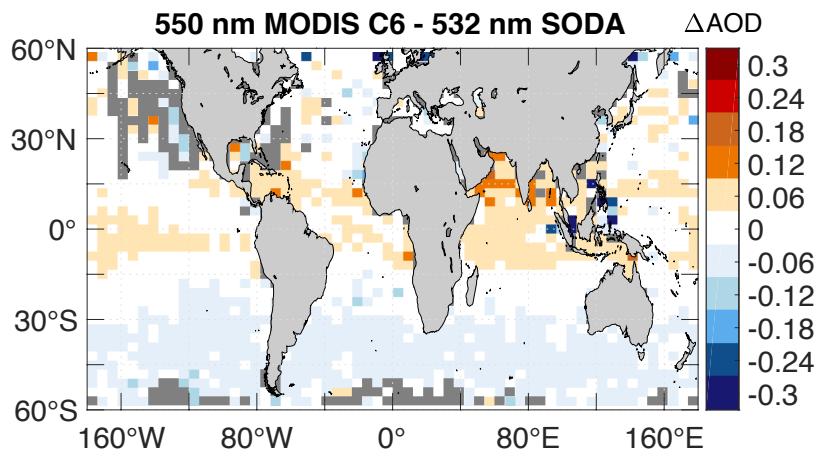


7



1 Figure 12: Fraction of daytime AOD contributed by the marine boundary layer.

2



3

4

Figure 13: Mean AOD difference between matched 550 nm MODIS C6 and 532nm SODA
daytime AOD for five months of 2010.

5

6

7

8

9

10

11

12

13

14

15

16

17

18

19

20

21

22

23



1

2 **Tables**

3

4

5

6 Table 1: Linear correlation coefficient (r), mean bias, and RSME between HSRL and SODA and

7 CALIOP Standard V4 AOD. Percentages are calculated relative to the mean HSRL AOD.

CALIOP-based AOD	r	Mean bias	RSME
SODA	0.96	-0.024 (-17%)	0.035 (24.2%)
Standard V4	0.94	0.014 (10%)	0.044 (31.2%)

8

9 Table 2: As in Table 1 but for CALIOP-SODA lidar ratio

CALIOP SODA LR	r	Mean bias	RSME
1 layer (1L)	0.67	-2.4 sr (-8.1%)	7.4 sr (24.8%)
2 layer (2L)	0.74	-3.9 sr (-12.5%)	8.1 sr (26.0%)

10

11 Table 3: As in Table 1 but for V4 and SODA aerosol extinction coefficient in the lower troposphere

12 (below 3.0 km).

CALIOP-based extinction	r	Mean bias	RMSE
CALIOP V4	0.82	0.013 km ⁻¹ (33.0%)	0.043 km ⁻¹ (106.0%)
SODA 1 layer (1L)	0.78	-0.0037 km ⁻¹ (-9.2%)	0.028 km ⁻¹ (72.6%)
SODA 2 layer (2L)	0.79	-0.0029 km ⁻¹ (-7.0%)	0.028 km ⁻¹ (73.8%)

13